AFRL-VS-TR-2003-1541

MEASURING ELECTRODYNAMICS OF THE IONOSPHERE BY DIGITAL IONOSONDES AND OTHER HF TECHNIQUES

Bodo Reinisch
Gary Sales

University of Massachusetts Lowell
Center for Atmospheric Research
600 Suffolk Street
Lowell, MA 01854

20 January 2003

Final Report

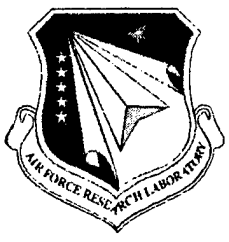

AIR FORCE RESEARCH LABORATORY
Space Vehicles Directorate
29 Randolph Rd
AIR FORCE MATERIEL COMMAND
HANSCOM AFB, MA 01731-3010

"This technical report has been reviewed and is approved for publication"

/signed/

GLEN MARPLE, SMSgt, USAF
Contract Manager

/signed/

ROBERT MORRIS
Branch Chief

This report has been reviewed by the ESC Public Affairs Office (PA) and is releasable to the National Technical Information Service (NTIS).

Qualified requestors may obtain additional copies from the Defense Technical Information Center (DTIC). All others should apply to the National Technical Information Service (NTIS).

If your address has changed, if you wish to be removed from the mailing list, or if the addressee is no longer employed by your organization, please notify AFRL/VSIM, 29 Randolph Road, Hanscom AFB MA 01731-3010. This will assist us in maintaining a current mailing list.

Do not return copies of this report unless contractual obligations or notices on a specific document require that it be returned.

REPORT DOCUMENTATION PAGE

Form Approved
OMB No. 0704-0188

1. REPORT DATE *(DD-MM-YYYY)*	2. REPORT TYPE	3. DATES COVERED *(From - To)*
20-01-2003	Scientific, Final	24 Sep 1996-23 Sep 2002

4. TITLE AND SUBTITLE
Measuring Electrodynamics of the Ionosphere by Digital Ionosondes and Other HF Techniques

5a. CONTRACT NUMBER
F19628-96-C-0159

5b. GRANT NUMBER

5c. PROGRAM ELEMENT NUMBER
62601F

6. AUTHOR(S)
Bodo Reinisch
Gary Sales

5d. PROJECT NUMBER
1010

5e. TASK NUMBER
IC

5f. WORK UNIT NUMBER
AA

7. PERFORMING ORGANIZATION NAME(S) AND ADDRESS(ES)
University of Massachusetts Lowell
Center for Atmospheric Research
600 Suffolk St
Lowell, MA 01854

8. PERFORMING ORGANIZATION REPORT NUMBER

9. SPONSORING/MONITORING AGENCY NAME(S) AND ADDRESS(ES)
Air Force Research Laboratory/VSBX
29 Randolph Road
Hanscom AFB, MA 01731-3010

10. SPONSOR/MONITOR'S ACRONYM(S)

11. SPONSOR/MONITOR'S REPORT NUMBER(S)
AFRL-VS-TR-2003-1541

12. DISTRIBUTION/AVAILABILITY STATEMENT
Approved for Public Release; distribution unlimited.

13. SUPPLEMENTARY NOTES

14. ABSTRACT
We conducted a general investigation into radiowave propagation modeling and ionospheric structure in the equatorial region. Techniques were developed to track ionospheric bubbles that form after sunset at or near the magnetic equator. These bubbles were identified as a source of satellite scintillation at 250 MHz. Drift speeds averaging around 100 m/s were observed during the test period in South America. HF propagation on a global scale was modeled using the USAF PRISM model of the ionosphere and rapid ray tracing techniques. These were combined with absorption and noise models to generate operational HF performance maps. Data bases combining global ionosonde measurements were established for the calibration andvalidation of satellite borne ionospheric measurements. As part of this program, special ionogram scaling and processing techniques were developed for auroral-E traces often observed at high latitudes.

15. SUBJECT TERMS
Ionosphere, Equatorial bubbles, Satellite scintillation, Instabilities, Auroral E layer, UV electron density measurements, OpSEND, UPOS

16. SECURITY CLASSIFICATION OF:			17. LIMITATION OF ABSTRACT	18. NUMBER OF PAGES	19a. NAME OF RESPONSIBLE PERSON
a. REPORT	b. ABSTRACT	c. THIS PAGE			Glen Marple, SMSgt, USAF
UNCL	UNCL	UNCL	UNL		19b. TELEPHONE NUMBER *(Include area code)* 781 377-3151

CONTENTS

FIGURES

TABLES

1. INTRODUCTION

This report summarizes the five years of AFRL supported research on the characteristics and structure of the ionosphere as it impacts the operational requirements of the US Air Force. Three major areas of our research: equatorial scintillation, OpSEND and Calibration/Validation of DMSP UV measurements are addressed in this report. We also include a description of the extensive support effort directed towards the operational facilities of the Air Force.

2. EQUATORIAL SCINTILLATION

2.1 Introduction

It is well established that on many days, after sunset, the equatorial F-region becomes unstable, resulting in amplitude and phase disturbance of trans-ionospheric satellite signals. The principal problem here is to determine which days will be effected and which will remain undisturbed. This prediction problem involves the understanding of the trigger mechanism and the conditions necessary for the rapid growth of these Rayleigh-Taylor (R-T) instabilities. This project involves analysis of scintillation phenomena using one year's satellite scintillation data from Ancon, Peru (Jicamarca). Two geostationary satellites were used. These satellites transmit at a frequency of about 250 MHz. One is over the Pacific Ocean to the west of Ancon and another is over the Atlantic Ocean to the east. The intersection of the line-of-sight path from the satellites to Ancon through the F-region is shown in Figure 1. Figure 1 also shows for a second

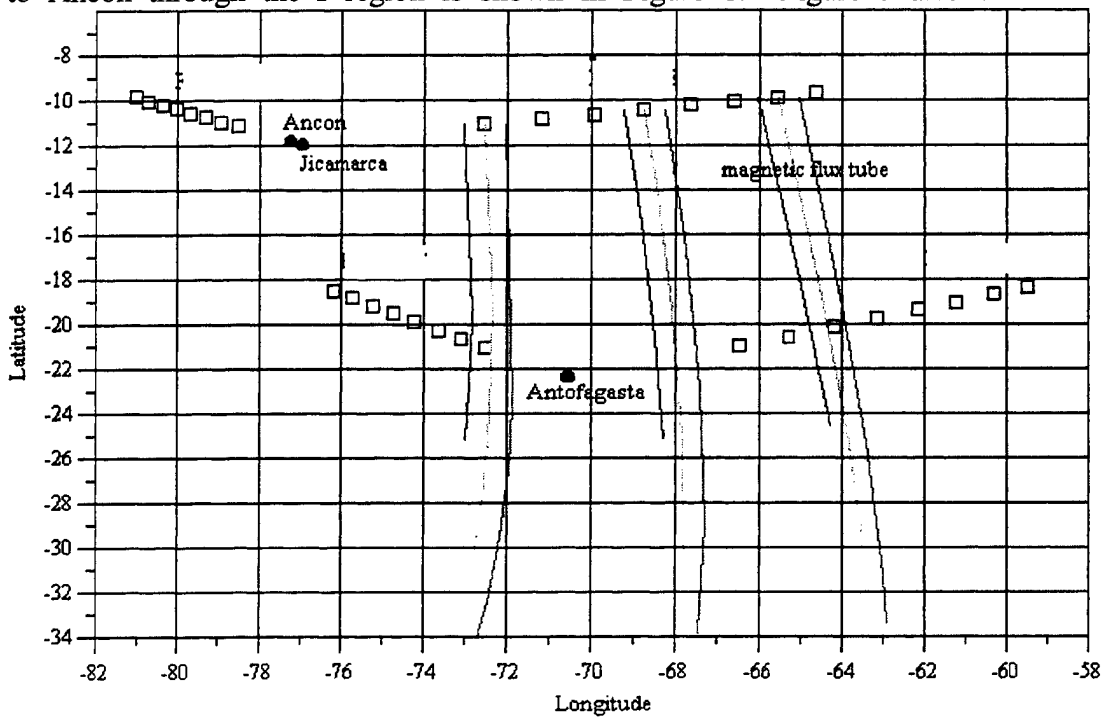

Figure 1. Location of the Ionospheric Sub-Satellite Points from the Atlantic and Pacific Satellites are shown as a function of altitude from 300 to 900 km. The near vertical curves show the magnetic flux tubes aligned along the local magnetic meridian in this region.

receiving station at Antofagasto, Peru, near the southern anomaly region, the ionospheric intersection points from the same two satellites. The indicated points show the intersection location as a function of height, from 300 to 900 km altitude.

The system at Ancon continuously records each satellite signal, and the scintillation index S4 was used to indicate the presence of scintillations. Scintillations typically begin within one hour after sunset and can continue for many hours during the night. Along with the scintillation measurements, the DPS ionospheric sounder at Jicamarca was operated on a one half hour schedule during the year. These routine sounder measurements and ionogram inversions made it possible to follow density and height variations that are associated with the onset of scintillation. After sunset, spread-F on the ionograms appears as the dominant feature associated with scintillation. This investigation attempts to develop the relationship between the early stages of spread-F and the development of full-blown scintillation.

2.2 Scintillation Statistics

Scintillation begins after F-layer (300 km) sunset, typically from 30 minutes to 90 minutes after the F-layer is no longer illuminated. Figure 2 combines all the data from the two satellites to show the onset time of scintillation (S4 > 0.6) relative to the F-layer sunset for the entire year of 1998.

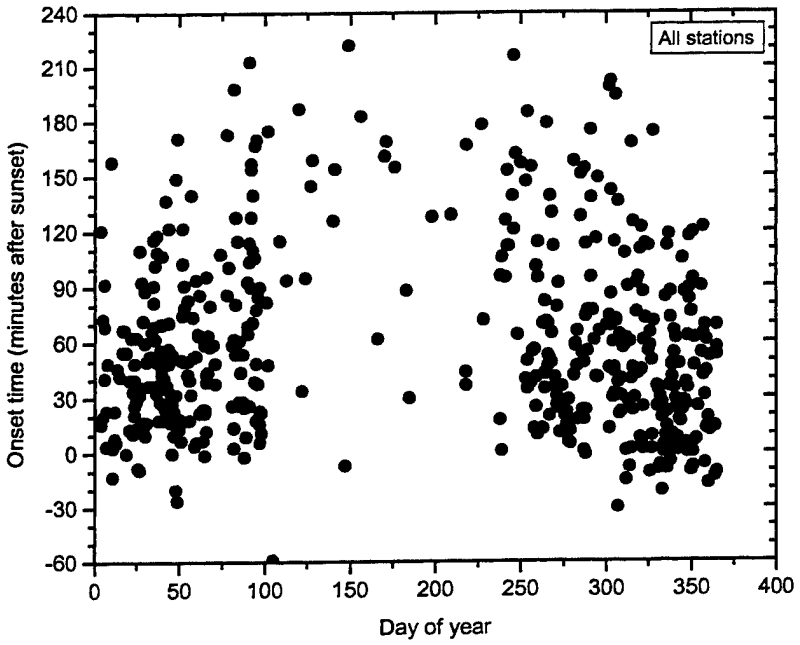

Figure 2. Occurrence of scintillation relative to sunset at Ancon using geostationary satellites for 1998.

Two factors become obvious from these data. First, between day 100 and 240 (approximately April through August) the occurrence of strong scintillation is relatively rare. This is a well-known characteristic, though the period of minimum scintillation occurrence varies with geographic location, apparently depending on the local magnetic declination. The second factor is best examined using the histogram (Figure 3) of the onset times for all these data, excluding days 100 through 240.

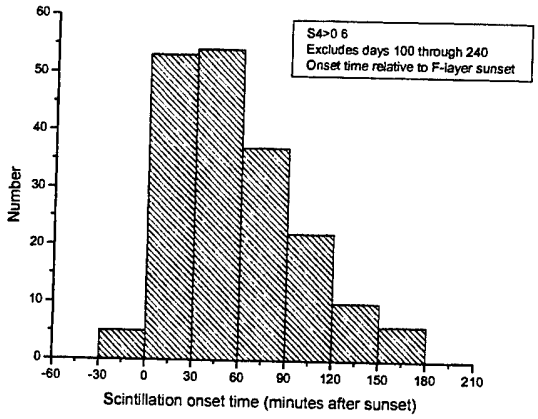

Figure 3. Histogram of the onset time relative to sunset for strong scintillation at Ancon for the year 1998 (all days except 100 through 240).

The majority of these data lie between 0 and 60 minutes after F-layer sunset with a median value, based on the entire distribution, of 48 minutes. Time delays a long as three hours were observed and less than five percent of the events occurred before sunset. As will be discussed later in this report, the growth factor for the R-T instabilities depends primarily on the character of the F-region ionization near the bottom of the layer. The first look at the changes in the height of the bottom of the layer was shown to give a good prediction of the onset of scintillation with a lead-time of one to two hours. This was based on the enhanced vertical movement of the F-layer that begins just before sunset. This movement, an ***ExB*** vertical drift velocity, is connected to changes in the zonal electric field. Figure 4 shows the virtual height changes of the F-layer for the months of October, November, and December 1998. These results followed the height variations using a sounding frequency of 5 MHz. It was important to use a frequency that reflects from the F-region during the entire day. Although there appears to be consistency during the daytime period, this changes approximately one hour before sunset when the virtual reflection height begins to rise. Clearly, the height change varies considerably during this pre-reversal period of height increase, the F-layer maximum height reaching a virtual height of 500 to 600 km on some nights and changing only a small amount on others.

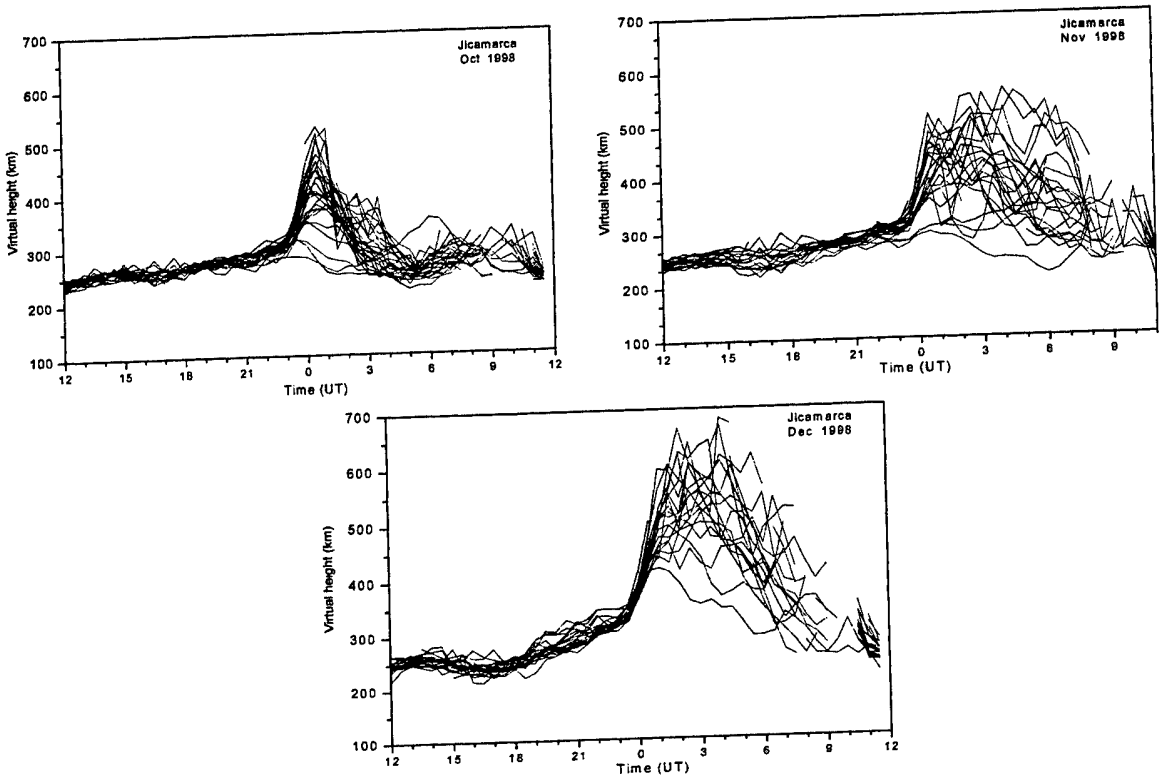

Figure 4. Jicamarca virtual height variation at 5 MHz for Oct., Nov. and Dec., 1998

Statistically, these data can be combined with the S4 index by showing the probability to predict the occurrence of scintillation before it begins. Figure 5 plots the time averaged scintillation index against the peak altitude for a 40-night period from 1 Feb.1997 to 31 March 1997. Here, these data are divided at S4 = 0.4 and virtual height = 400 km. The choice of 400 km, by coincidence, divides the data set into two equal parts. However, for given $z_{peak} < 400$ km, the probability of scintillation is 0.20, while for $z_{peak} > 400$ km, the probability of scintillation rises to 0.85. These are conditional probabilities that do not have to sum to unity.

Referring to Figure 4, the layer very typically reaches 400 km at F-layer sunset, when it does reach 400 km, giving a mean prediction lead-time of 48 minutes. This means that near layer sunset, if the height of the F-layer is greater than or equal to 400 km, then the probability of scintillation is 85 percent.

The other important statistic is that if spread-F is observed on any given evening after sunset, the occurrence of scintillation is 100 percent. Clearly, spread-F is a precursor to scintillation. This is of little predictive value since the time difference between these occurrences is typically less than 30 minutes.

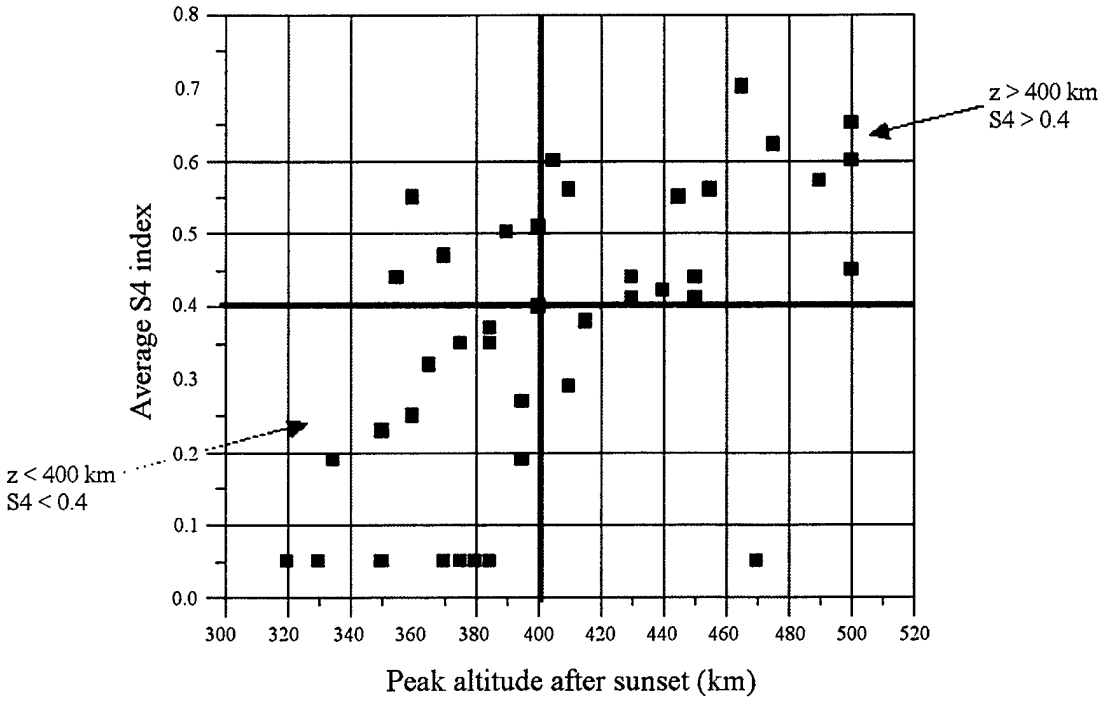

Figure 5. Distribution of nightly S4 events as a function of peak F-layer virtual height.

2.3 Instability Motions

These R-T instabilities drift eastward after they are formed with the ***ExB*** drift associated with the downward electric field at an average speed of 100 m/s. Analysis of many Jicamarca ionograms indicated that the sounder could detect the large bubbles before they reached the overhead position and, in a sense, the bubbles could be tracked as they approached the sounder location. Unfortunately, the Jicamarca sounder ran on a 30-minute schedule that limits its ability to precisely determine the drift speed. A sequence of ionograms is shown in Figure 6, beginning at 00 UT (F-layer sunset). The bubble instability reaches the overhead position at 0200 UT.

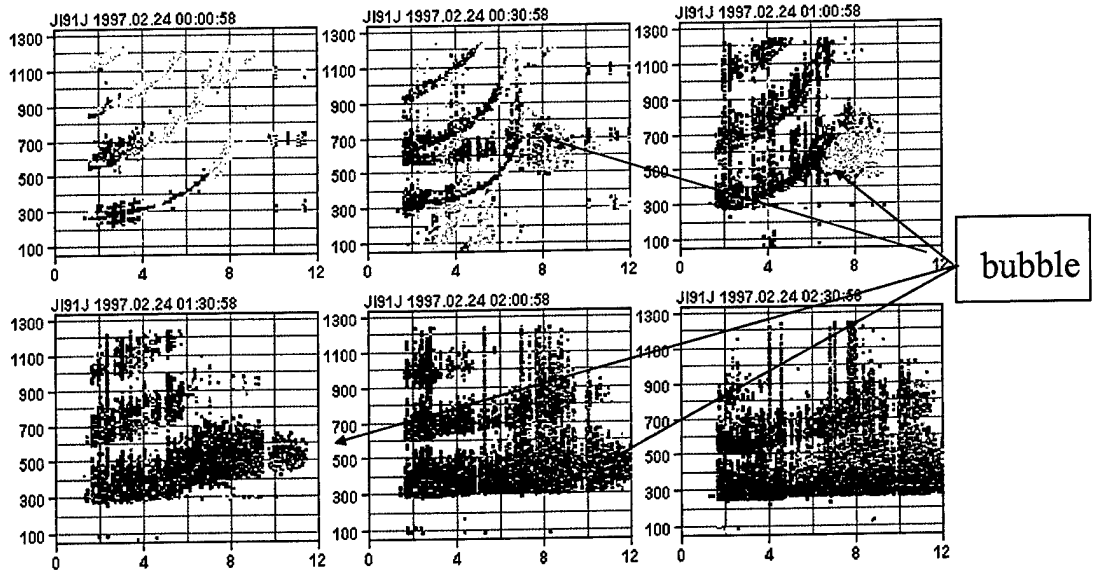

Figure 6. Jicamarca ionograms sequence from 24 February 1997 showing the approach of the bubble region.

Combining the sounder data, the Julia radar and the scintillation index give a composite picture of the equatorial phenomenology during this sunset period, as shown in Figure 7. The Julia radar at the Jicamarca radar facility is a subset of the incoherent scatter radar that operates at lower power. At this level it is able to detect only the stronger coherent scatter components of

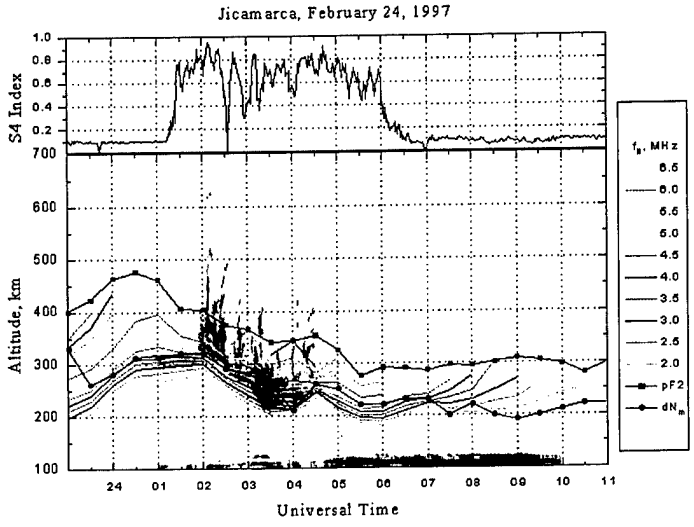

Figure 7. Composite of ionosonde true height contours, the Julia radar and scintillation index.

irregularity structure passing over Jicamarca. However, the lower power requirement allows the Julia radar to operate on a more frequent basis and is used here to compare with the digisonde data. Superimposed on the plasma frequency contours derived from the ionogram inversions for the 24-hour period are the Julia radar data and plotted above is the Ancon scintillation index for satellite. On the basis of these data, the radar shows that bubbles originates near the bottom of the layer, specifically, very close to the to the region of maximum electron density gradient as shown by the diamond symbol trace. This is associated with the R-T instability growth factor as discussed in the next section. The Julia radar scatter grows to heights above the peak of the F-layer. In this example, the bubble structures arrive over Jicamarca at around 0200 UT, with bottom-side spread-F beginning approximately one hour earlier. The scintillation appears to begin with the appearance of bottom-side spread-F but it must be remembered that the ionospheric intersection point of the scintillation lies to the west of Jicamarca and more closely coincides with the bubble's passage before it reaches the overhead position.

Figure 8 illustrates the relationship between the bubble's eastward drift and the several measuring techniques used here. Three-dimensional numerical ray tracing was used to understand how the sounder is able to image the approaching bubbles before they reach the overhead position. The model of the bubble (a columnar region depleted of 90 percent of the ambient ionization and reaching from the bottom of the F-layer through the peak of the layer) was superimposed on the PRISM ionospheric model. The ray tracing was carried out at 7 MHz for several positions of the bubble region with respect to the sounder location (Jicamarca).

These calculations show the existence of many points inside each bubble where the ray is orthogonal with the local magnetic field indicating the potential for scatter back to the sounder. On the basis of these calculations it expected that the sounder is just able to detect the approaching bubbles at a maximum range of 500 km and more easily as the bubbles get closer to Jicamarca.

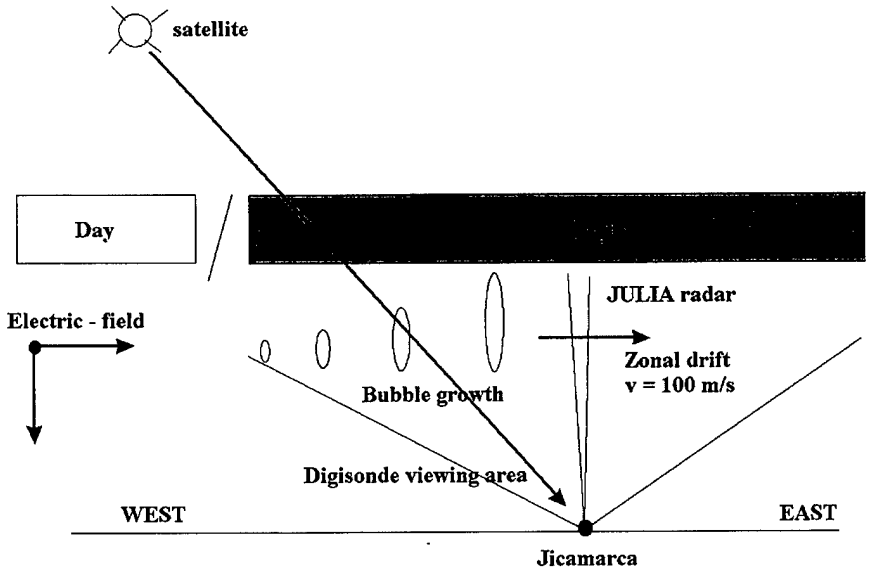

Figure 8. Illustration of the relationship between eastward drifting but es and the several measurement techniques.

Finally, for several nights the tracking of the bubbles by the sounder was used to determine the eastward drift velocity. These measurements are shown in Figure 9, plotting location against time.

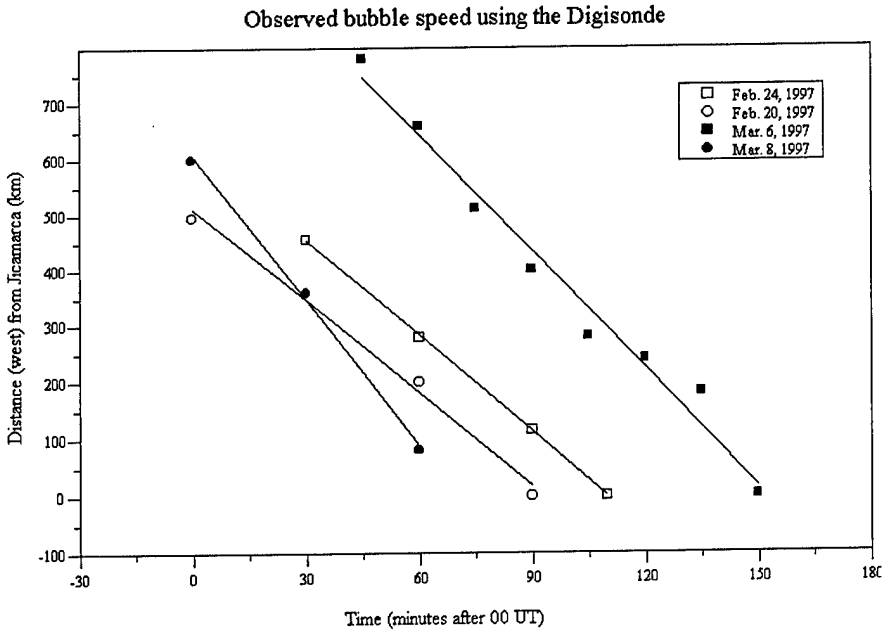

Figure 9. Observed distance of equatorial bubbles from Jicamarca as a function of time on four nights.

The average speed varied from 80 to 140 m/s on these days.

Following Kelley [1989] the R-T instability growth factor is expressed below in terms of the zonal electric field intensity E_x, the geomagnetic field B, the acceleration of gravity g, the ion-neutral collision frequency ν_{in} and the layer tilt angle τ.

$$\gamma_{RT} = \frac{1}{L}\left[\frac{E_x}{B}\cos(\tau) + \frac{g}{\nu_{in}}\cos(\tau) + \frac{E_x + uB}{B}\sin(\tau)\right] \quad (s^{-1}) \tag{1}$$

The length scale L is given in terms of the electron density profile as $L = \left[\frac{1}{n_e}\frac{dn_e}{dz}\right]^{-1}$. (2)

The largest instability growth rate occurs when L is minimum or where dn/dz is largest. In general, this occurs near the bottom of the F-layer. Future research involves determining from each measured electron density profile where the minimum L occurs and the magnitude of L at that point. For simplicity, if the layer tilt angle is assumed to be zero, then the third term, containing sin (τ), is zero and the resultant expression becomes:

$$\gamma_{RT} = \frac{1}{L}\left[\frac{E_x}{B} + \frac{g}{\nu_{in}}\right] \quad (s^{-1}) \tag{3}$$

The remaining important factors are the magnitude of the zonal electric field and the ion-neutral collision frequency that decreases with increasing height of the F-layer. This explains the increasing probability of scintillation occurrence as the layer is driven upward around sunset. The zonal electric field then plays an important dual role. First, directly in the equation of the growth rate and second, in driving the layer upward, thereby decreasing the ion-neutral collision frequency. Both effects work to increase the instability growth rate. The measurement of the zonal electric field (vertical ***ExB*** drift) is discussed in Section 4 and the ion-neutral collision frequency is available from the sounder electron density measurements and the MSIS neutral atmospheric model.

2.4 Drift Analysis

On the basis of the above analysis on the R-T instability growth rate, the most important factor is the upward drift of the layer beginning just before sunset. The Digisonde in the "drift mode" is able to measure a vertical drift velocity. Radio sounding measurements of vertical drift has two components. The first is the motion of the reflection point, which depends on the sounding frequency, as the layer moves upward (or downward) and the second component is the time dependent change in the electron content below the reflection level that introduces a velocity component. This analysis starts with two equations listed below: the continuity equation for electrons (the same for ions assuming charge neutrality and only a single ion species: O^+) and the phase path derivative (Doppler frequency).

Where the phase path P is:

$$\frac{\partial n_e}{\partial t} + \nabla \cdot (n_e \mathbf{v}) = Q - L$$
$$\delta f = -\frac{1}{\lambda}\frac{dP}{dt} \tag{4}$$

$$P(t) = \int_0^{zr(t)} \mu(z,t)\,dz \tag{5}$$

where:

$$\mu^2 = 1 - \frac{80.6\,n_e}{f_o^2} \tag{6}$$

and z_r is the reflection height.

Combining these two equations for the vertical component of the motion leads to the equation for the vertical plasma drift velocity:

$$v_z = \frac{v_d + \frac{k}{2f^2}\int_{z_o}^{z_R}\frac{1}{\mu}(Q-L)\,dz}{\frac{k}{2f^2}\int_{z_o}^{z_R}\frac{1}{\mu}\frac{\partial n}{\partial z}\,dz} \qquad where: \quad v_d = -c\frac{\delta f}{f} \tag{7}$$

in terms of the sounder drift velocity v_d, the solar ionization production rate Q and the electron loss rate L.

This is an important equation relating the vertical plasma drift velocity with the sounder measured, Doppler derived, vertical velocity measurement. Analysis of this equation is planned for future efforts. Using models of solar flux as a function of wavelength and ionization loss models it will be possible to compare the derived plasma drift with the incoherent scatter radar measurements.

3. PERFORMANCE OF HF COMMUNICATION SYSTEMS

3.1 Introduction

Two programs, OpSEND and UPOS, have been designed to predict the expected HF performance of operational HF communications and radar systems, respectively. As inputs, the two programs use the PRISM ionospheric model that is updated at any time based on real-time measurements from a variety of sensors. These include ionospheric sounders, total electron content measurements and DMSP satellite measurements of particle fluxes that specifically affect the character of the auroral ionosphere. Based on our earlier work, reported extensively in the Annual Report 2000 that involved the development of both programs, OpSEND and UPOS model the performance of HF communications systems at any location by generating wide-area signal-to-noise maps that operators can use to assess their ability to illuminate a remote site at any particular frequency. These performance calculations combine a rapid 2-D ray-tracing technique called SMART, developed by DERA in the United Kingdom with the USAF PRISM ionospheric model.

3.2 OpSEND and UPOS

There are differences between the two programs. OpSEND is a one-way communication simulation programmed to hypothetical receivers located anywhere on a latitude/longitude grid, in all directions around a specified transmitter site. These programs include all losses including geometrical spreading, D-region absorption as well as a frequency/time dependent noise model (atmospheric, manmade and galactic). The program computes signal strength, and signal-to-noise ratio at each grid point location. The second program, UPOS, simulates the performance of an HF backscatter radar system. This requires a two-way path from the radar to the remote ground cell and then scatter back to the radar. This requires an additional parameter for the ground backscatter coefficient. The UPOS program, as developed here, involved only the ground backscatter component, although the actual HF radar (SuperDARN) that was used to compare results was primarily employed as a detector of backscatter from field-aligned ionospheric irregularities.

The OpSEND program was delivered to USAF and installed for operational use in the year 2000. Although the OpSEND product appeared to work well, there was no independent check on the effectiveness of the performance prediction. On the other hand, with the UPOS program, it was possible to validate the approach used in these simulations by comparing performance predictions with actual radar measurements. The difficulty imposed by the UPOS program was that high latitude ionosphere was involved in these comparative tests. The

SuperDARN radar operated by the University of Alaska on Kodiak Island was the available high latitude HF radar system used here for the comparative measurements. This radar scans continuously over Alaska looking at both ionospheric scatter from irregularities in the E and F-layers and ground scatter after the radar energy reflects from the ionosphere and backscatters from the "rough" ground. For the UPOS study, it was the ground scatter that the program attempts to simulate.

USAF PRISM provided the ionospheric models used in all the simulations, both operational and for validation. The PRISM model provides a latitude/longitude grid of electron density profiles over the globe where the appropriate section covering the desired area for OpSEND is selected by the operator and over the Alaskan region for UPOS. The results of these efforts are described in considerable detail in the Annual Report 2000 and only this brief review is included here although considerable effort was expended on these projects. A typical example of the OpSEND operational performance map is included here to illustrate the scope of the effort.

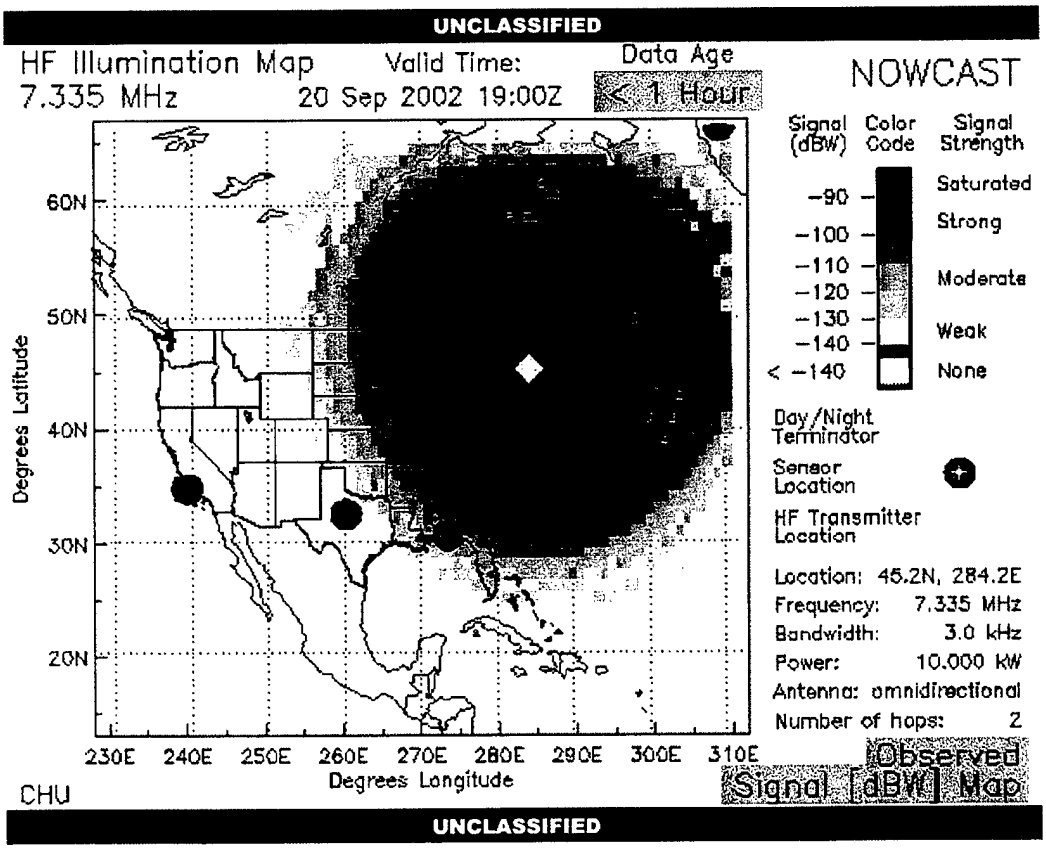

Figure 10. Typical HF Illumination Map – for a transmitter located near Ottawa, Canada transmitting at 7.335 MHz with a 10 kW transmitter. The darker shades of gray represent increasing received signal power (dBW).

This map was generated for 20 Sept. 2002 at 1900 UT, which is daytime over the area shown. The signal falls off with distance from the transmitter indicating a useable range of about 1500 km in the daytime. This service range would increase at night with a skip zone surrounding the transmitter. The OpSEND and UPOS programs handle all this.

4. CALIBRATION/VALIDATION OF SATELLITE BORNE UV ELECTRON DENSITY MEASUREMENTS

Two far-ultraviolet (FUV) remote sensing instruments are planned to fly on future DMSP 5D3 (Defense Meteorological Satellite Program) satellites. One is the Special Sensor Ultraviolet Spectrographic Imager, or SSUSI (http://www.cpi.com/projects/ssusi.html), which will make disk and limb observations of auroral emission, dayglow, and nightglow. The other is the Special Sensor Ultraviolet Limb Imager, or SSULI, (http://www.pxi.com/praxis_publicpages/SSULI.html) designed to measure the natural airglow radiation from atoms, molecules, and ions in the upper atmosphere and ionosphere. Ionospheric electron density profiles in the auroral E region and in the F region are expected data products.

Calibration and/or validation of this space borne UV technique with established and proven techniques are required. It was decided to use the electron density profiles available from the worldwide network of digisondes (Figure 11) for this calibration/validation effort.

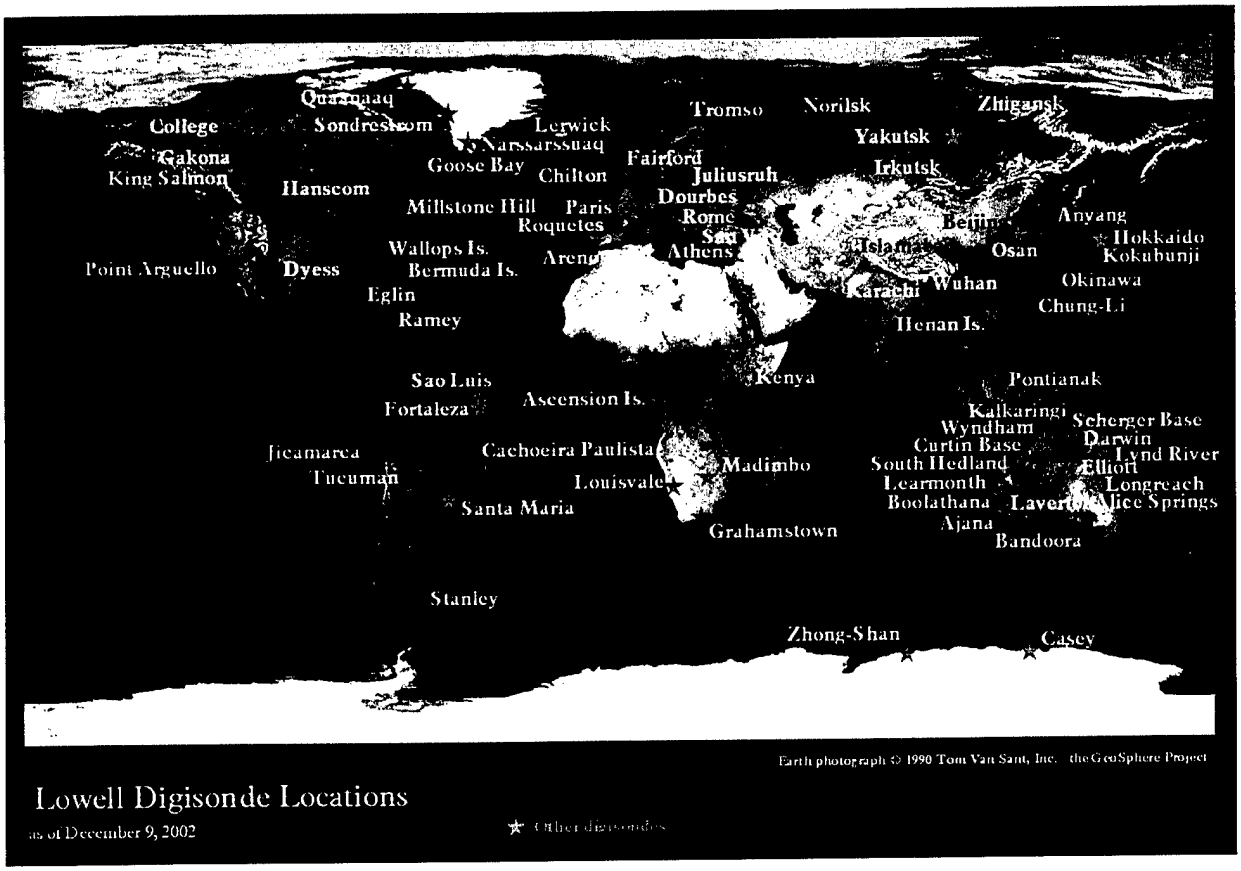

Figure 11. The digisonde network

4.1 Digital Ionogram Data Base (DIDBase)

A new information system has been developed that actively manages data from the distributed digital ionosonde network in support of a variety of ionospheric modeling and comparison projects. As a result of the progress in interactive data processing technologies, database management, remote control, and networking solutions, for the first time a working environment has been created that accesses the wealth of automatically scaled and manually validated ionospheric data derived from ionograms. With the digisonde data roster in mind, DIDBase is expandable to support other ionosonde models that use the universal Standard Archival Output (SAO) format for ionospheric characteristics, and the non-specific Binary Large OBject (BLOB) technology to store the source ionogram data. Inspired by the SPIDR (Space Physics Interactive Data Resource) Web project, developed and maintained by the WDC-A, the DIDBase expands the database features to allow storage of the binary ionograms together with multiple scaling records for each ionogram. By relaxing the conventional scenario "one ionogram – one set of derived characteristics", the DIDBase creates new possibilities for multiple trace identifications, storage of alternative ionogram interpretations, and a variety of comparative studies of the automated ionogram processing quality. In particular, the new technology made it possible to store several simultaneously observed auroral E layers, which is of special interest to high latitude ionospheric research. To provide end users with fast access to the best ionogram interpretation results, the DIDBase reduces all versions of ionogram scalings to a single subset of characteristics using a hierarchy of expert ratings and quality flags. The new information system includes the "Digital Ionogram Data Base" (DIDBase), the expert ionogram scaling software tool "SAO Explorer", and the "Automated Data Request Execution Subsystem" (ADRES) to manage specialized data requests and monitor their status from the inception to the final report.

To compare ionospheric measurements made from the ground with satellite measurements, it is important to enhance the cadence of ground observations during times when the sub satellite point is close to the ground station. During routine operation, many of the digisondes operate at a 15 min or 30 min cadence, some at 60 min. During satellite passes over a digisonde station, the cadence must increase to one ionogram every 5 min for about one hour. Based on the satellite orbit predictions, the operating schedule of the 38 digisondes around the globe participating in the "CAL/VAL" effort must be adjusted to the higher cadence for the duration of the passes, in cooperation with the station owners/operators. Table 1 shows the list of the currently activated CAL/VAL stations. We have obtained permission to use the data from these stations and to change their modes of operation.

Table 1. DIDBase Active Digisonde Stations

DIDB Active Station List for 2002

	URSI code	NAME		URSI code	NAME
1.	AS00Q	ASCENSION ISLAND	18.	KS759	KING SALMON
2.	AT138	ATHENS	19.	LV12P	LOUISVALE
3.	BV53Q	BUNDOORA	20.	MHJ45	MILLSTONE HILL
4.	CAJ2M	CACHOEIRA PAULISTA	21.	OK426	OKINAWA
5.	RL052	CHILTON	22.	SN437	OSAN AB
6.	CO764	COLLEGE AK	23.	PSJ5J	PORT STANLEY
7.	DB049	DOURBES	24.	PA836	PT ARGUELLO
8.	DS932	DYESS AFB	25.	THJ77	QAANAAQ
9.	EG931	EGLIN AFB	26.	PRJ18	ROME
10.	EA036	EL ARENOSILLO	27.	EB040	ROQUETES
11.	FF051	FAIRFORD, UK	28.	VT139	SAN VITO
12.	FZA0M	FORTALEZA	29.	SAA0K	SAO LUIS
13.	GSJ53	GOOSE BAY	30.	SMJ67	SONDRESTROM
14.	GR13L	GRAHAMSTOWN	31.	TR169	TROMSO
15.	HA419	HAINAN	32.	WP937	WALLOPS IS
16.	JI91J	JICAMARCA	33.	WU430	WUHAN
17.	JR055	JULIUSRUH			

Also available: Anyang, Gakona, Kokubunji, Tucuman, Ramey

A total of approximately 60,000 ionograms is expected for a one-month CAL/VAL period. This data volume requires the development of a "digital ionogram database or DIDBase, with direct access," to SAO-Explorer, the fourth generation tool for digisonde data visualization SAO-X. DIDBase was developed in consultation with Terence Bullett of AFRL, and is briefly described below. A second requirement is a mechanism that automatically reads incoming requests from the satellite operators and adjusts programs and schedules of the Internet-enabled digisondes. SAO-X was upgraded to include the ADRES subsystem to handle this task.

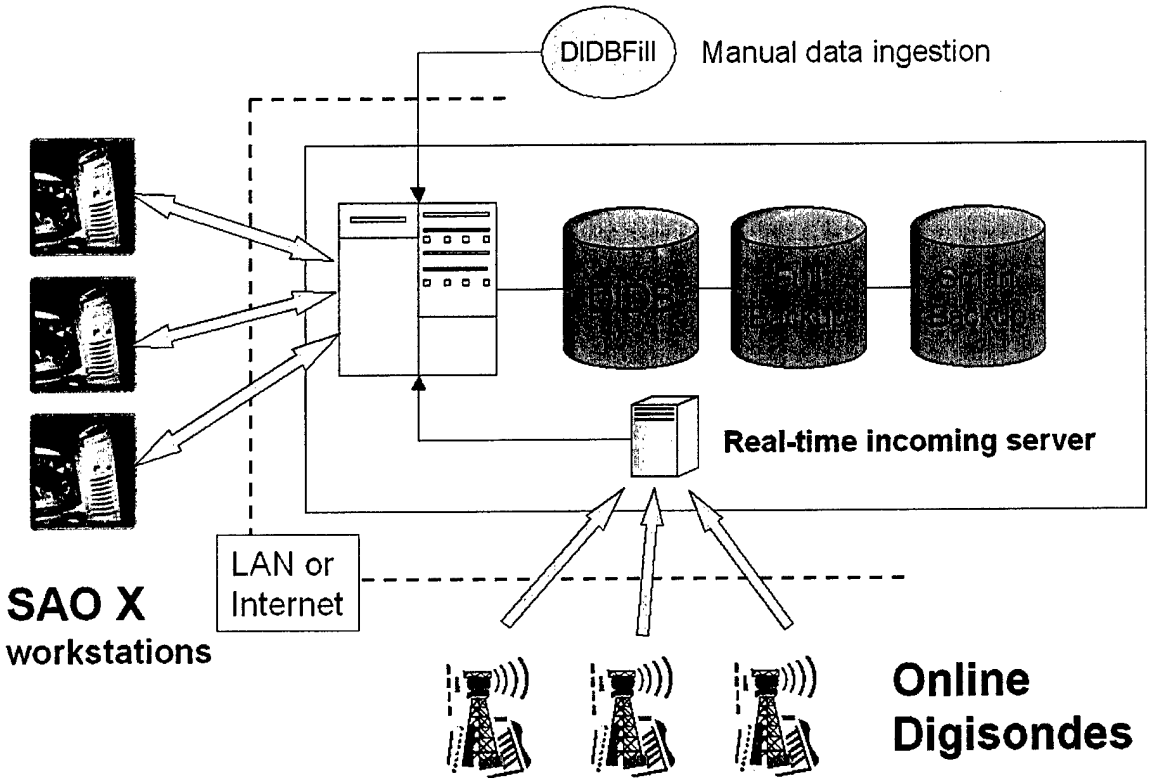

Figure 12. Organization of DIDBase

Figure 12 shows the organization of the data flow for the CAL/VAL operation. The digisonde data are deposited in the database, and the SAO-X workstations have direct access to these data. This is important since the ARTIST autoscaling of ionograms [Reinisch and Huang, 1983] is not always error free, and manual editing of the scaling is required to assure correct electron density profiles for comparison with the UV results. Two examples of autoscaled ionograms from Jicamarca for 5 Dec 2002 are shown in the left column in Figure 13. The autoscaling at 2100 UT (upper panel) is very accurate with values of 14.2 MHz and 419 km for foF2 and hmF2. Manual editing (right column) changed these values by only ~1%, although the calculated vertical total electron content (TEC) changed by 5%. At 2315 UT ARTIST was misled by a small echo gap in the trace (possibly caused by interference) and grossly underestimated foF2, hmF2, and TEC, as can be seen in the edited ionogram on the right. While ARTIST has been slightly improved since this record was made to avoid hanging up on small gaps, these mistakes are still occurring for the DISS stations where the AF Frequency License creates wide gaps in the traces.

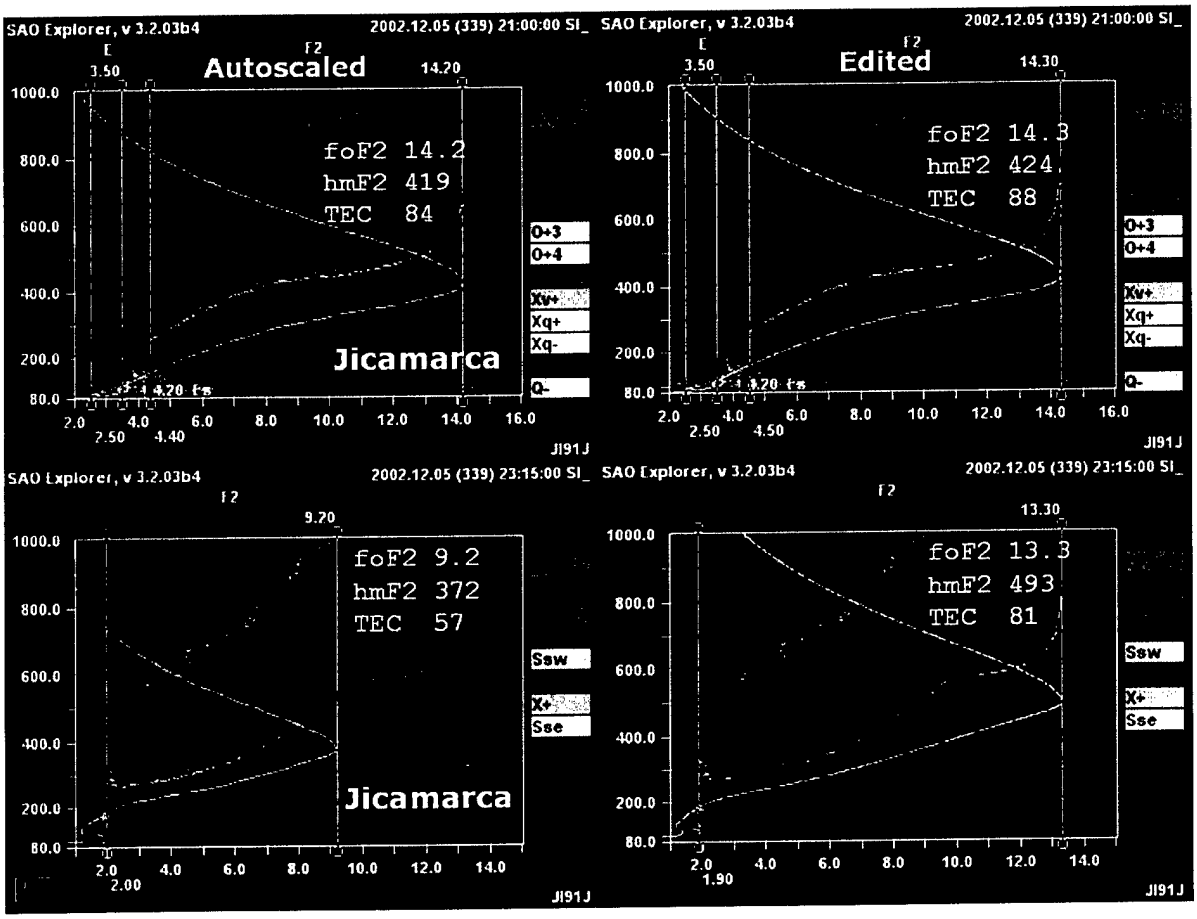

Figure 13. Illustrating the need for manual editing

The function of the ADRES subsystem is illustrated in Figure 14. ADRES consists of two Java based programs, DIDBFill (loading data into DIDBase) and DIDBReqPro (DIDBase Request Processor). The ADRES subsystem can request validated ionospheric data in form of plain text reports. If the requested data are already in DIDBase and had been validated, the ADRES generates the report immediately. A provision is made to manage the requests for special modes of ionosonde operation (e.g., high ionogram rate during a satellite pass over the station, a coordinated campaign, or an event of interest) and data that are not available in DIDBase or are not manually validated. The ADRES has a mechanism to automatically read incoming requests to adjust programs and schedules of the Internet-enabled Digisondes. To acquire Digisonde data, the ADRES maintains a list of FTP servers where the ionogram data can be found. A number of digisonde stations deliver their real time data directly to a WDC and to DIDBase. As soon as the data are ingested, a message is generated to the SAO-X operators to validate/edit the autoscaling results. When the quality control procedure is completed, the final report is generated and delivered to the requesting party.

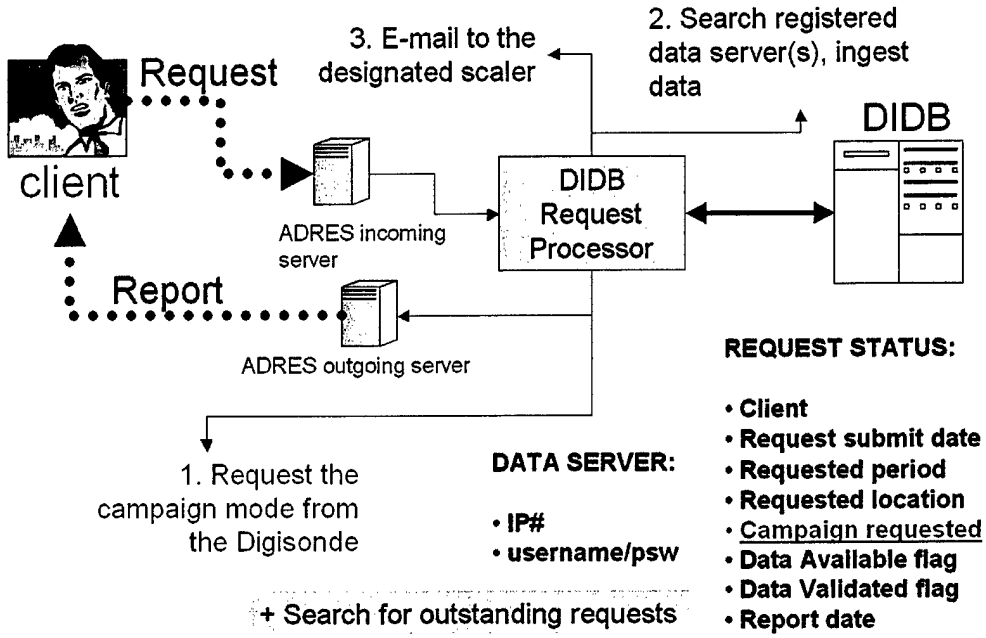

Figure 14. The functions of the DIDBase ADRES subsystem

4.2 CAL/VAL Dry Run with TIMED/GUVI

The TIMED spacecraft carries a UV instrument, GUVI, which is almost identical to the SSUSI instrument to be flown on DMSP. A real time dry run was initiated for the TIMED spacecraft orbit during a 3-day campaign from 25-27 April 2002 to test and exercise the DIDBase/digisonde network operation. Ionospheric model predictions for this magnetic storm period were compared with the characteristics measured by the digisondes at 11 stations in the Western hemisphere (Table 2).

Table 2. Eleven digisonde stations were included in the TIMED dry run

#	URSI CODE	STATION NAME
1	WP937	Wallops Island
2	DS932	Dyess
3	AS00Q	Ascension Island
4	MHJ45	Millstone Hill
5	JI91J	Jicamarca
6	PSJ5J	Port Stanley
7	SAA0K	SAO LUIS
8	CAJ2M	CACHOEIRA PAULISTA
9	FZA0M	Fortaleza
10	EG931	Eglin
11	PA836	Pt Arguello

Model simulations (gray) of the diurnal variations of the F2 layer peak density and height are shown in Figure 15 for six digisonde locations. The measurements are shown as black curves.

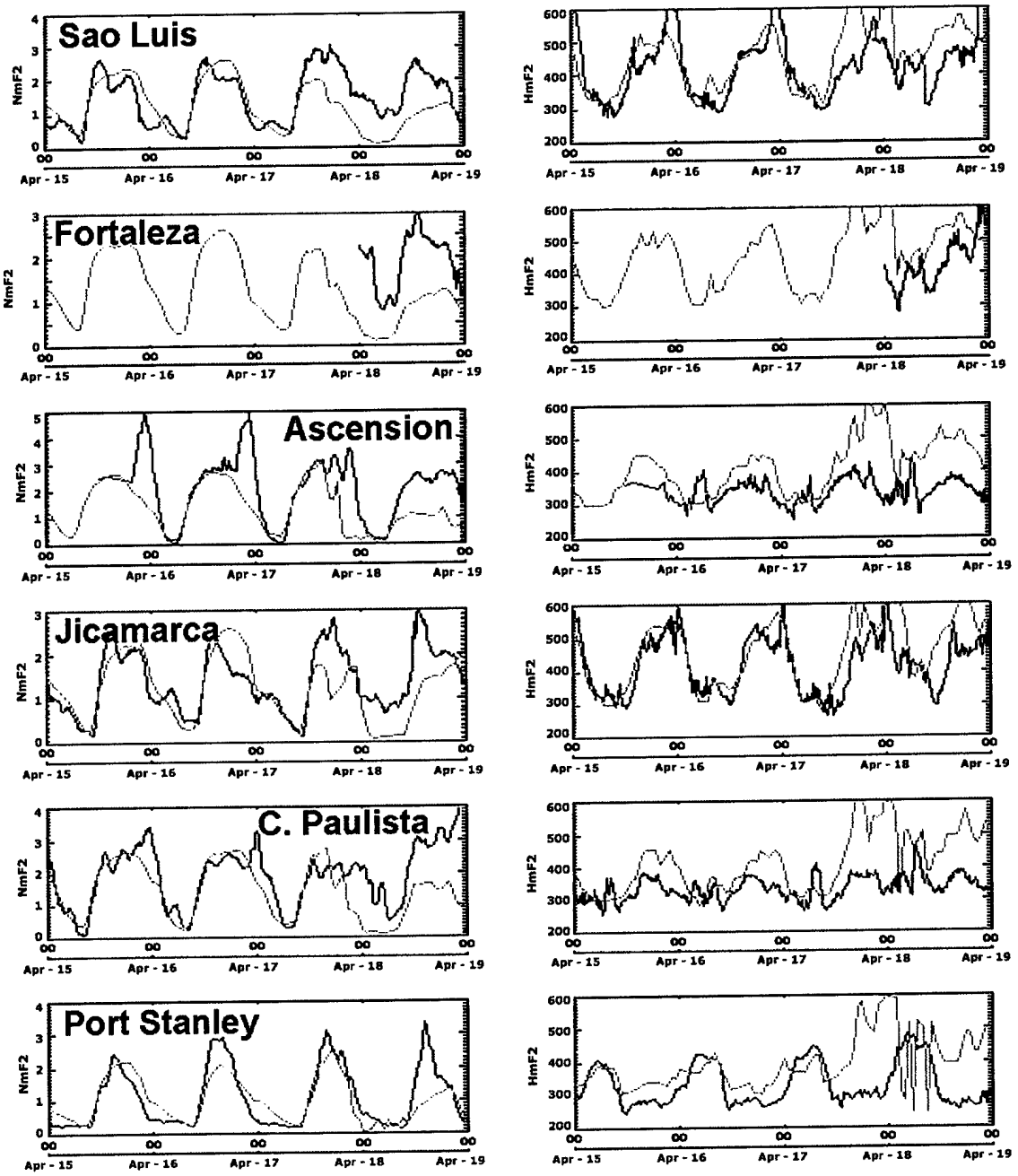

Figure 15. Simulations (gray) of NmF2 (cm^{-3} x 10^{-6}) on the left and hmF2 (km), on the right, for the Southern hemisphere, are compared with digisonde measurements (black). (courtesy of Paul Straus, Aerospace Corporation)

The digisonde software (both DPS-4 and DGS-256) has been modified so that it automatically responds to CAL/VAL campaign requests. Requests received from Aerospace are entered into the ADRES system to automatically reprogram the sounding schedule and

measurement programs of selected stations. A request example for 25 April 2002 is shown in Table 3 (all times are given in UT).

Table 3. Request for CAL/VAL campaign

```
ADD
WP937, 2002.04.25 21:09:00, 2002.04.25 22:09:00
DS932, 2002.04.25 00:05:00, 2002.04.25 01:05:00
AS00Q, 2002.04.25 17:43:00, 2002.04.25 18:43:00
MHJ45, 2002.04.25 21:11:00, 2002.04.25 22:11:00
JI91J, 2002.04.25 20:56:00, 2002.04.25 21:56:00
PSJ5J, 2002.04.25 17:28:00, 2002.04.25 18:28:00
PSJ5J, 2002.04.25 19:08:00, 2002.04.25 20:08:00
SAA0K, 2002.04.25 19:21:00, 2002.04.25 20:21:00
CAJ2M, 2002.04.25 19:16:00, 2002.04.25 20:16:00
FZA0M, 2002.04.25 19:21:00, 2002.04.25 20:21:00
```

ADRES also issues text reports to Aerospace containing the most relevant measurements (an example is given in Table 4). Starting in late 2002, these reports used the standard SAO-4 data format (http://129.63.134.1/framesd.htm)

Table 4. CAL/VAL campaign request for the Millstone Hill digisonde

UMass Lowell Ionospheric REPORT REQUESTED BY DMSP Space Science Applications Laboratory The Aerospace Corporation

```
FOR STATION: MILLSTONE HILL, URSI: MHJ45
START TIME: 2002-Apr-26 (116) 21:29:00 UT
END TIME: 2002-Apr-26 (116) 22:29:00 UT
Auto scaled - A, Validated - V, TEC units - [10^16 m^-2]
```

yyyy.MM.dd	(DDD)	HH:mm:ss	A/V	foF2 [MHz]	hmF2 [km]	TEC [TECU]	foEa [MHz]
2002.04.26	(116)	21:30:00	V	9.750	308.0	32.5	---
2002.04.26	(116)	21:35:00	V	9.750	307.6	32.2	---
2002.04.26	(116)	21:40:00	V	9.750	307.6	31.6	---
2002.04.26	(116)	21:45:00	V	9.750	307.8	31.2	---
2002.04.26	(116)	21:50:01	V	9.850	314.3	33.3	---
2002.04.26	(116)	21:55:00	V	9.850	311.5	32.2	---
2002.04.26	(116)	22:00:00	V	9.850	309.9	31.2	---
2002.04.26	(116)	22:05:00	V	9.950	312.7	32.6	---
2002.04.26	(116)	22:10:00	V	9.950	313.2	32.7	---
2002.04.26	(116)	22:15:00	V	9.850	307.9	30.0	---
2002.04.26	(116)	22:20:00	V	9.950	312.7	31.9	---
2002.04.26	(116)	22:25:00	V	9.950	309.0	30.0	---

4.3 Auroral E Layer Studies at Sondrestrom

It is planned to deduce the E region electron density profiles from the nighttime SSUSI measurements. Of special interest will be the ionization produced by electron precipitation in the auroral zone. This ionization also shows on ionograms in the form of auroral E layers, as illustrated in Figure 16. Enhanced retardations of the echoes occur at 1.7 MHz, 5.2 MHz, and 5.8 MHz, indicating ionization peaks within the field of view of the digisonde's antenna system. With a beam width of approximately 1 radian, an area of 50 km radius at E region heights contributes to the ionograms. This area contains regions of higher density, 3.3×10^{11} and 4.2×10^{11} m^{-3}, and the background ionization of 3.6×10^{10} m^{-3}. At times when only a single auroral-E layer is present, it is likely to be associated with diffuse aurora. The footprint of the SSUSI instrument is about a factor of 2 smaller than the digisonde's, but it still will contain significantly varying densities.

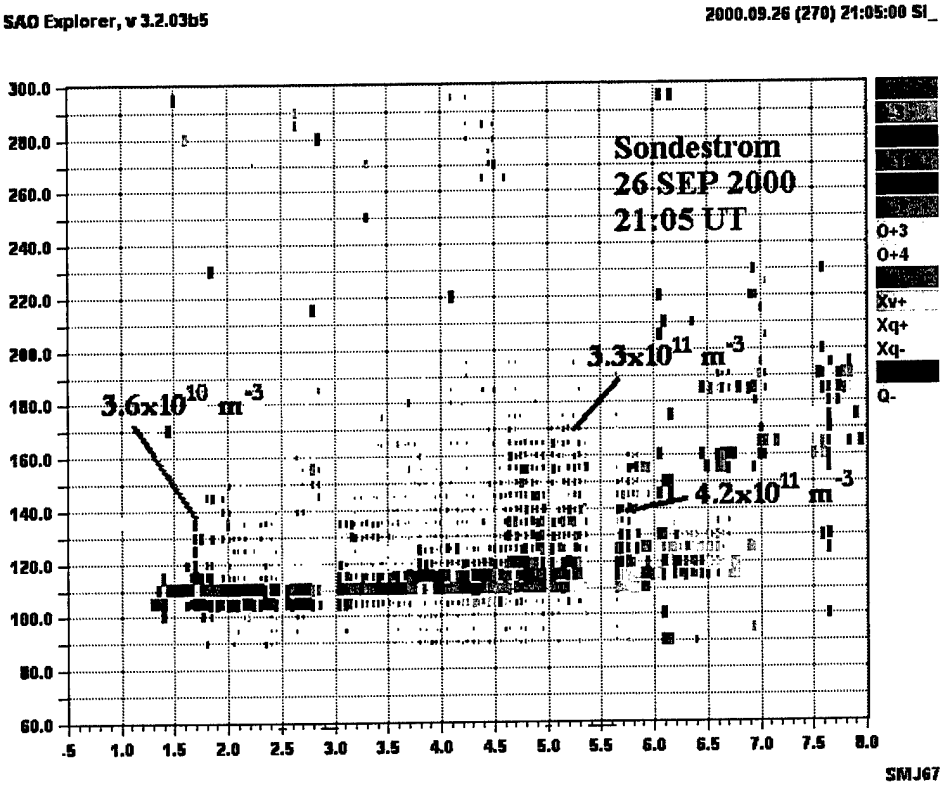

Figure 16. E region ionograms at Sondrestrom on 26 Sep 2000 at 2105 UT. The data gaps at 2.9 MHz and 5.4 MHz are caused by transmission restrictions in the AF Frequency License

The collocated incoherent scatter radar at Sondrestrom was making profile measurements during this time in a fixed beam direction parallel **B**. The ISR beam width is 0.6° corresponding to a 1 km footprint in the E region. The one-minute sequence of ISR profiles displayed in Figure 17 shows an order of magnitude variation in N_mE. The digisonde measurements of N_mE from the ionogram at 2105 UT were added to the figure. While the digisonde "sees" all densities at once, the ISR sees the blobs of ionization move through its beam as function of time.

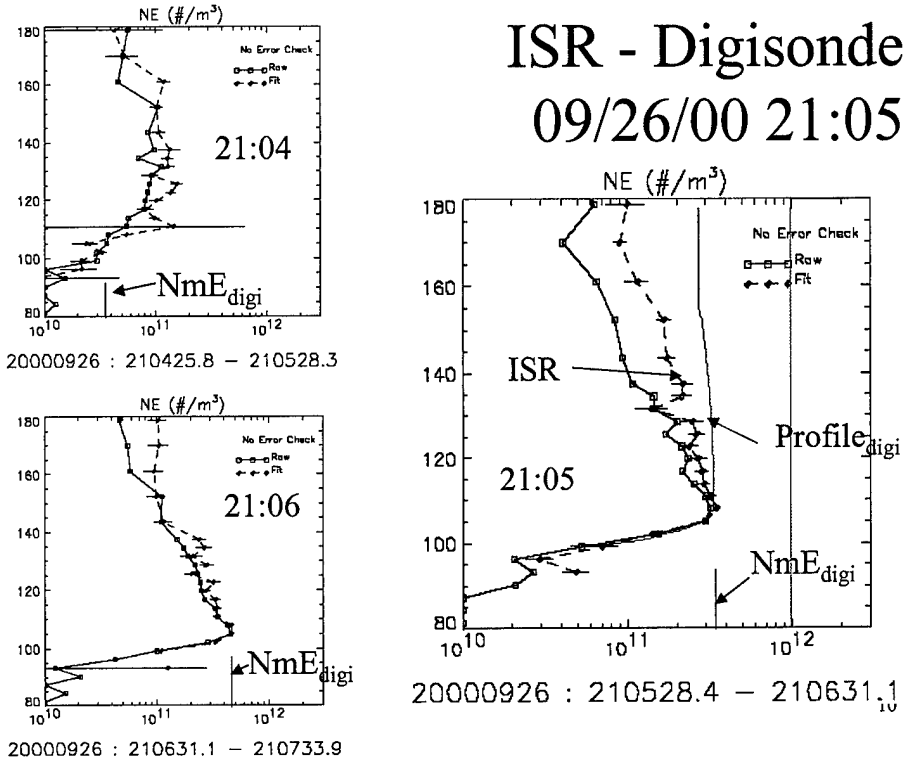

Figure 17. One-minute sequence of incoherent scatter radar electron density profiles (black) at Sondrestrom. One digisonde profile from the 2105 UT ionograms is shown in red, superimposed on the 2105 UT ISR profile. Two other peak densities (red marker) from the 2105 UT ionograms are shown on the profiles with similar N_mE. (ISR profiles courtesy Jeff Thayer, SRI).

5. LIST OF PUBLICATIONS

The following publications in refereed journals were generated under this research contract.

Sales, G.S., B. W. Reinisch, J. L. Scali, C. Dozois, T. W. Bullett, E. J. Weber, and P. Ning, Spread-F and the structure of equatorial ionization depletions in the Southern Anomaly Region, *J. Geophys. Res.*, **101**, A12, 26,819-26,827, 1996.

Huang, X. and B.W. Reinisch, Vertical electron density profiles from the digisonde network, *Adv. Space Res.*, **18**, 6, (6) 121-(6)129, 1996.

Reinisch, B.W. and X. Huang, Low latitude digisonde measurements and comparison with IRI, *Adv. Space Res.*, **18**, 6, (6) 5-(6) 12, 1996.

Reinisch, B.W. and X. Huang, The F1 region at 170 km, *Adv. Space Res.*, **18**, 6, (6) 153-(6) 156, 1996.

Colerico, M., M. Mendillo, D. Nottingham, J. Baumgardner, J. Meriwether, J. Mirick, B.W. Reinisch, J.L. Scali, C.G. Fesen, and M.A. Biondi, Coordinated measurements of F region dynamics related to the thermospheric midnight temperature maximum, *J. Geophys. Res.*, **101**, A12, 26,783-26,793, 1996.

Huang, X. and B.W. Reinisch, Vertical electron density profiles from digisonde ionograms. The average representative profile, *Annali di Geofisica*, **XXXIX**, 4, 751-756, 1996.

Galkin, I.A., B.W. Reinisch, G.A. Osokov, E.G. Zazobina, and S.P. Neshyba, Feedback neural networks for ARTIST ionogram processing, *Radio Sci.*, **31**, 5, 1119-1128, 1996.

Scali, J.L., and B.W. Reinisch, Geomagnetic storm time studies using Digisonde data, *Adv. Space Res.*, **20**, 9, 1679-1688, 1997.

Reinisch, B.W., D.M. Haines, K. Bibl, I. Galkin, X. Huang, D.F. Kitrosser, G.S. Sales, and J.L. Scali, Ionospheric sounding support of OTH radar, *Radio Sci.*, **32**, 4, 1681-1694, 1997.

Mendillo, M., J. Baumgardner, D. Nottingham, J. Aarons, B.W. Reinisch, J.L. Scali, and M. Kelley, Investigations of thermospheric-ionospheric dynamics with 6300-Å images from the Arecibo Observatory, *J. Geophys. Res.*, **102**(A4), 7331-7343, 1997.

Reinisch, B.W., Modern Ionosondes, in Modern Ionospheric Science, (Eds. H. Kohl, R. Ruster, and K. Schlegel), European Geophysical Society, 37191 Katlenburg-Lindau, Germany, 440-458, 1996.

Reinisch, B.W., Ionosondes, in Upper Atmosphere (Eds. Dieminger, W., Hartmann, G.K., Leitinger, R.), Springer, 370-381, 1996.

Radicella, S.M., D. Bilitza, B.W. Reinisch, J.O. Adeniyi, M.E. Mosert Gonzalez, B. Zolesi, M.L. Zhang, and S.R. Zhang, IRI Task Force Activity at ICTP: Proposed improvements for the IRI region below the F peak, *Adv. Space Res.*, **22**, 6, 731-739, 1998.

Reinisch, B.W. and X. Huang, Finding better B_0 and B_1 parameters for the IRI F2-profile function, *Adv. Space Res.*, **22**, 6, 741-747, 1998.

Reinisch, B.W., J.L. Scali, and D.M. Haines, Ionospheric drift measurements with ionosondes, *Annali di Geofisica*, **41**, N. 5-6, 695-702, 1998.

Valladares, C.E., R. Sheehan, D.T. Decker, D.N. Anderson, T. Bullett, and B.W. Reinisch, Formation of polar cap patches with north-to-south transitions of the interplanetary magnetic field, *J. Geophys. Res.*, **103**, A7, 14,657-14,670, 1998.

Anderson, D.N., M.J. Buonsanto, M. Codrescu, D. Decker, C.G. Fesen, T.J. Fuller-Rowell, B.W. Reinisch, P.G. Richards, R.G. Roble, R.W. Schunk, and J.J. Sojka, Intercomparison of physical models and observations of the ionosphere, *J. Geophys. Res.*, **103**, A2, 2179-2192, 1998.

Reinisch, B.W., 'CHARS': URSI IIWG format for archiving monthly ionospheric characteristics, *INAG Bulletin No. 62*, WDC-A for STP, Boulder, CO, 38-46, 1998a.

Reinisch, B.W., SAO (Standard ADEP Output) format for ionogram scaled data archiving, *INAG Bulletin No. 62*, WDC-A for STP, Boulder, CO, 47-58, 1998b.

Reinisch, B.W., Radio Sounding of Geospace Plasmas, *Fisica de la Tierra*, **12**, 105-126, 2000.

Sales, G. S., Reinisch, B.W., Paznukhov, V., and Hysell, D.L., Equatorial Bubble Development and the Source of Satellite Scintillations, ISEA Proceedings-10, 2000.

Crowley, G., Ridley, A.J., Deist, D., Wing, S., Knipp, D.J., Emery, B.A., Foster, J., Heelis, R., Hairston, M., and Reinisch, B.W., Transformation of high-latitude ionospheric F-region patches into blobs during the March 21, 1990 storm, *Geophys. Res.*, **105**, A3, 5215-5230, 2000.

Richards, P.G., Buonsanto, M.J., Reinisch, B.W., Holt, J., Fennelly, J.A., Scali, J.L., Comfort, R.H., Germany, G.A., Spann, J., Brittnacher, M., Parks, F.K., and Fok, M.-C., On the relative importance of convection and temperature on the behavior of the ionosphere in North America during Jan, 6-12, 1997, *J. Geophys Res.*, **105**, A6, 12, 763-12, 776, 2000.

Reinisch, B. W., Huang, X., Deducing Topside Profiles and Total Electron Content from Bottom side Ionograms, *Adv. Space Res.*, **27**, 1, 23-30, 2001.

Huang, X., Reinisch, B. W., Bilitza, D., IRI in Windows Environment, *Adv. Space Res.*, **27**, 1, 127-131, 2001.

Huang, X., Reinisch, B. W., Vertical Electron Content from Ionograms in Real Time, *Radio Sci.*, **36**, 2, 335-342, March/April 2001.

Reinisch, B.W., Haines, D.M., Sales, G.S., Benson, R.F., Green, J.L., Taylor, W.W.L., Radio sounding in space: magnetosphere and topside ionosphere, *J. Atmos. Solar-terr. Phys.*, **63**, 87-98, 2001.

Stephan, A.W., Colerico, M., Mendillo, M., Reinisch, B.W., and Anderson, D., Suppression of equatorial spread F by sporadic E, *J. Geophys. Res.*, **107**(A2), 10.1029/2001JA000162, 2002.

Fesen, C.G., Hysell, D.L., Meriwether, J.W., Mendillo, M., Fejer, B.G., Roble, R.G., Reinisch, B.W., Biondi, M.A., Modeling of low latitude atmosphere and ionosphere, *J. Atmos. Solar-Terr. Phys*, **64** (2002), 1337-1349, 2002.

6. SUPPORT

During the lifetime of this contract, the Center for Atmospheric Research (CAR) has provided extensive support to the USAF and its facilities around the world. Below is a list of the travel carried out by CAR as part of this support function.

9-13 Feb 1996	Bermuda
1-6 June 1996	Osan AB, Korea
11-17 Nov 1996	Tromso, Norway
17-21 Mar. 1997	RAF Fairford, UK
	USAF AWS/Space Forecast
	CLRC RAL
22-29 Sept. 1997	Sondrestrom, Greenland
21-22 Jan 1998	Wallops Island, VA
19 Feb-4 Mar 1998	McClellan, Vandenburg AFB, CA
21 Mar – 4 Apr. 1998	Korea
	Japan
28 Apr – 2 May 1998	Eglin AFB, FL
	Dyess AFB, TX
14-21 Aug 1998	Goose Bay, Canada
	Narsarsuaq, Greenland
28 Aug 1998	Wallops Island, VA
18 Sept. 1998	Goose Bay, Canada
23-25 Sept. 1998	Wallops Island, VA
28-29 Oct. 1998	Wallops Island, VA
15-20 Nov. 1998	Sacramento, CA
29 Nov – 2 Dec. 1998	Eglin AFB-Ft. Walton Beach, FL
29 Nov – 2 Dec 1998	Ramey Solar Observatory, San Juan, PR
28-31 Dec 1998	Bermuda
4-8 Jan 1999	Sheep Creek and Gakona, AK
27-31 Dec 1999	Bermuda
27-31 March 2000	Tobyhanna, PA
18-24 June 2000	Tobyhanna, PA
9-12 Oct. 2000	Bermuda

11-18 Mar. 2001	Ascension Island
4-6 March 2002	Wallops Island, VA
7-12 May 2002	HAARP – Gakona, AK
3-10 July 2002	Tucuman, Argentina
15-22 Sept. 2002	Campo Grande, Brazil

7. REFERENCES

Kelley, M. C., The Earth's Ionosphere, Plasma Physics and Electrodynamics, International *Geophysics Series*, **43**, 1989.

Reinisch, B. W. and Huang, X., Automatic Calculation of Electron Density Profiles from Digital Ionograms, 3, Processing of Bottomside Ionograms, *Radio Sci.*, **18**, 477, 1983.